Interference effects with surface plasmons

Kuzmin, N.V.

Chapter 4

Bouncing surface plasmons[1]

Employing an interferometric cavity ring-down technique we study the launching, propagation and reflection of surface plasmons on a smooth gold-air interface that is intersected by two parallel, sub-wavelength wide slits. Inside the low-finesse optical cavity defined by these slits the surface plasmon is observed to make multiple bounces. Our experimental data allow us to determine the surface-plasmon group velocity ($v_{\mathrm{group}} = 2.7 \pm 0.3 \times 10^{-8}$ m/s at $\lambda = 770$ nm) and the reflection coefficient ($R \approx 0.04$) of each of our slits for an incident surface plasmon. Moreover, we find that the phase jump upon reflection off a slit is equal to the scattering phase acquired when light is converted into a plasmon at one slit and back-converted to light at the other slit. This allows us to explain fine details in the transmission spectrum of our double slits.

[1]) N.V. Kuzmin, P.F.A. Alkemade, G.W. 't Hooft and E.R. Eliel, *Bouncing surface plasmons*, Opt. Exp. **15**, p. 13757 (2007)

4.1 Introduction

The observation by Ebbesen *et al.* [36] that a metal film that is perforated by a regular array of sub-wavelength holes transmits much more light than what is predicted by classical theory [37] has sparked a wide-ranging research effort into the physics of electromagnetic fields interacting with structured metal films. It is now broadly understood that surface plasmons (SPs) play a very important role in this transmission enhancement and this understanding has birthed a novel field of research commonly called "plasmonics". Possible applications of plasmonics can be found in microscopy [65], bio-sensing [66,67], nano-optics [68,69], nonlinear optics [70], cavity-QED [71] etc.

Although the transmission enhancement by surface plasmons in a metal hole array is dramatic, this 2D system is not optimal for studying the basic physics of scattering of EM radiation by perforations in metal films. Single sub-wavelength holes or slits in thin metal films provide more fundamental systems and their transmission has therefore received considerable attention, both theoretically and experimentally [72]. An elegant extension to these basic systems is provided by the double slit, well known from Thomas Young's landmark experiment; it has recently been shown that surface plasmons can give rise to a modulation of the transmission spectrum of the double slit [34, 35, 61, 73]. Furthermore, it has been reported that the spatial coherence of the light field behind such a double slit can be modified by the surface plasmons [74,75]. In this type of experiments the sub-wavelength slit acts as an antenna — it scatters the incident radiation field into (Fig. 4.1a): i) a forward propagating field with emission angles ranging from $-\pi/2$ to $+\pi/2$; ii) a surface plasmon field travelling away from the slit along the metal-dielectric interface; iii) evanescent modes. A second, nearby slit can act as a receiver for the surface plasmon field and scatter it into, e.g., free space or into a backward-travelling/transmitted plasmon (Fig. 4.1b).

Incident light, that is coherently scattered into a plasmonic mode by one of the slits, can be re-radiated by the other slit, with a well-defined phase relationship with the light that is forward scattered by the latter slit; this explains the observed wavelength modulation of the transmission spectrum of the double slit [61].

A different perspective on this modulation is that it represents the eigenmode spectrum of the metallic resonator bounded by the two slits [76]. The near vicinity of metallic regions at the other side of each slit will have an effect on this spectrum; in a way they "dress" the resonator. The measured spectrum is then actually the extinction spectrum of the dressed inter-slit metallic 2D cavity [77]. This spectrum arises due to the multiple interference of waves

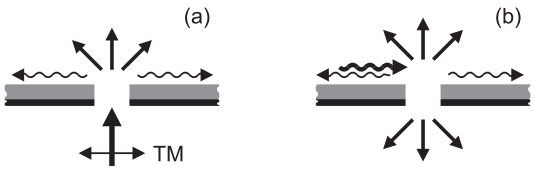

Figure 4.1. (a) The coupling of incident TM-polarized light into surface plasmons propagating along the metal-dielectric interface on top, accompanied by direct transmission; (b) Incident surface plasmon outcoupling to free-propagating light, back-reflection and tunneling through the slit. Bottom interface is covered with metal (Ti) that suppresses surface plasmon propagation.

that travel up and down the cavity, displaying sharp structure when the waves make many round trips through the resonator, and shallow features when the number of round trips is small (of order 1). In conventional optical resonators this number depends on the loss per round trip [78]. There are two contributions to this loss: internal loss due to extinction during propagation through the resonator (usually small or negligible in conventional optical resonators), and loss due to the finite mirror reflectivity or to diffractive losses at the edges of the mirror [78]. Both types of loss apply to our metallic resonator.

Here we report on time-domain measurements of the decay of the surface plasmon as it travels up and down a mesoscopic metallic resonator defined by sub-wavelength slits. These measurements yield data on the surface-plasmon group velocity, the reflection coefficient of a surface plasmon for a sub-wavelength slit, and on phase jumps upon scattering and reflection.

4.2 Experiment

A conventional optical resonator is characterized by two parameters, namely the cavity round-trip time $t_{\mathrm{ax}} = L/v_{\mathrm{group}}$ and the cavity decay time $\tau_{\mathrm{cav}} = -t_{\mathrm{ax}}/\ln(R)$, with R the mirror reflectivity. The former measures the time it takes a pulse to make a round trip through the cavity of length L, while the latter equals the $1/e$ decay time of the intracavity power. The equivalent parameters in the frequency domain are the free spectral range $\omega_{\mathrm{ax}} = 2\pi/t_{\mathrm{ax}}$ and the *finesse* $\mathcal{F}$; the finesse measures the ratio of the free spectral range and the cavity linewidth. Round-trip losses are the dominant factor that determine the finesse, and in conventional stable optical resonators the round-trip loss is usually determined by the reflectivity of the mirrors.

In the system under study, i.e., a resonator for surface plasmons, the round-

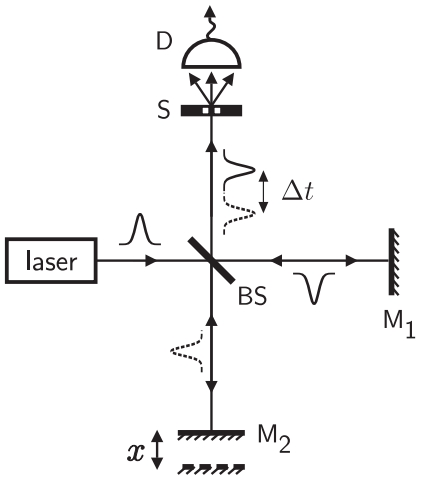

Figure 4.2. Experimental interferometer setup. The output of a wavelength tunable ultrashort pulsed Ti:sapphire laser, $\lambda = 770$–800 nm, is incident on a 50/50 beamsplitter (BS). The light reflects from two broadband dielectric mirrors (M_1,M_2) and is recombined at the beamsplitter. Behind the sample (S) the light is detected by a Si photodiode detector (D). The pump-probe delay is varied by moving mirror M_2.

trip losses are not only determined by the slit reflectivity but also by damping of the surface plasmon as it travels between the slits, due to the finite conductivity of the metal film. By a judicious choice of the cavity length L we can tune the ratio of these two loss mechanisms. Measurements of the spectrum of a surface-plasmon resonator consisting of a smooth metal film bounded by two sub-wavelength slits demonstrate that its finesse is small ($\mathcal{F} \approx 2$) [61]. In that limit the finesse of a resonator is not a sensitive measure of the reflectivity as opposed to the case that the finesse is high, and requires experimental data with good signal-to-noise ratio. Note that if the finesse of a cavity is low it is not given by the well-known approximate expression $\mathcal{F} = \pi R^{1/2}/(1-R)$, but by $\mathcal{F} = \pi/\{\arccos[2R/(1+R^2)]\} \approx 2(1+4R/\pi)$. We therefore have chosen to measure in the time domain, essentially using a cavity ring-down technique [79].

While a surface plasmon in the near-infrared spectral region ($\lambda \approx 800$ nm) propagates along a flat and unstructured air-gold interface its amplitude decays over a length of order 100 μm [8,53]. Unless a gain medium is present [80], a SP cavity should have a length that is, at most, of that same order and, therefore, the cavity round-trip time will not be larger than a few hundred femtoseconds. For modest values of the cavity finesse, the SP cavity ring-down

time will be of that same order of magnitude. Because of this ultra-short time scale traditional cavity ring-down techniques, where the power leaking through one of the cavity mirrors is monitored in real time [79], are not suited to the case of a SP cavity. Upconversion and autocorrelation techniques [81] provide alternatives here; the latter is used in the present work.

As a sample we use a 200 nm thick plane gold film attached to a fused-quartz substrate by a 10 nm thick titanium adhesion layer. The film is perforated by two 50 μm long and 100 nm wide slits, separated by distances ranging from 25 to 90 μm. The titanium adhesion layer is strongly dissipative to surface plasmons [61]; consequently the SPs that we study here are those of the gold-air interface.

We illuminate the sample by the output of a Michelson interferometer which, in turn, is illuminated by a short-coherence-length femtosecond tunable Ti:sapphire laser (Fig. 4.2). We choose the polarization of the incident light to be perpendicular to the long axis of the slits (TM-polarization). The laser is operated at wavelengths around 770–800 nm, with a spectral width of $\approx$ 30–40 nm, yielding a coherence length $\ell_{\mathrm{coh}} \approx$ 16–20 μm. The Michelson interferometer serves to generate a time-delayed copy of the laser pulse and, together, these two pulses illuminate both slits of our sample. We image the double-slit output on a low-noise detector (New Focus model 2001-FS) and measure its output as a function of the delay Δt between the two pulses incident on the sample. We collect the data on a computer using a 24-bit A/D converter (National Instruments PCI 5911) while slowly changing Δt using a motorized translation stage (Newport model CMA-25CCCL). Note that our experimental approach is slightly unusual in that we send *both* the original pulse, henceforth called pump, *and* its copy, called probe, onto our sample, instead of illuminating the sample with just one of the pulses [82]. We have made this choice because of the large angular spread of the output of the sample, its low transmission (typically 10^{-6} for a spot size of 50 μm diameter) and considerations of signal to noise.

4.3 Results

Experimental interferograms recorded with the laser operating at $\lambda = 770$ nm are shown in Fig. 4.3. The upper frame shows the autocorrelation trace obtained in the absence of a sample, yielding information on the instrumental response function of our setup. At a pump-probe delay of $\approx$ 50 fs the signal is essentially constant and remains so when the delay is increased. The lower frame shows the measured interferogram as recorded in the presence of our

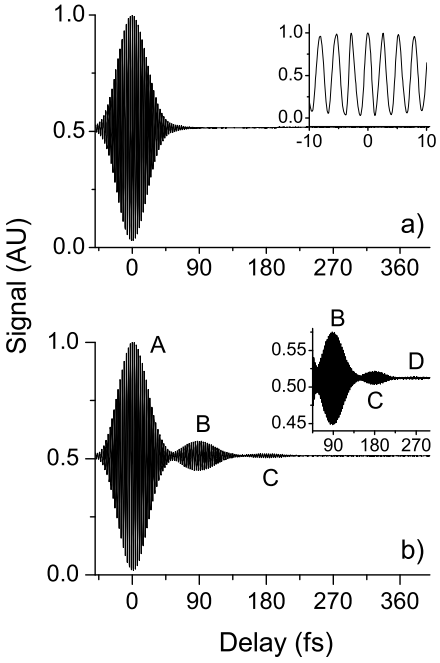

Figure 4.3. Experimental interferograms measured without sample (a) and with a sample containing a sub-wavelength slit pair with 25 μm slit separation (b). The insets show details of the interference signal.

sample, using a double slit with a slit separation of 25 μm and TM-polarized incident light. The interference fringes show a quite different behavior here: most noticeably one observes the signal to partially recover after the initial collapse (peak B, Fig. 4.3b). This "echo" has an amplitude of order 10% of the initial signal. Upon careful observation one notices that the signal goes through an additional cycle of collapse and recovery (peak C). When the polarization of the incident light is chosen to be TE, we observe no revivals; the signal is indistinguishable from that measured with the double slit absent (Fig. 4.3a).

As we will argue below, the first echo (B) comes about because surface plasmons are launched at the slits, travel from one slit to the other, to arrive there after a delay Δt; the second, weaker, echo (C) arises because a surface plasmon that is launched at one of the slits, can be back-scattered by the other slit to return to its place of birth with a delay equal to $2\Delta t$.

More detailed information on the sequence of echo's can be obtained by demodulating the signal of Fig. 4.3b to obtain its carrier envelope; the latter we

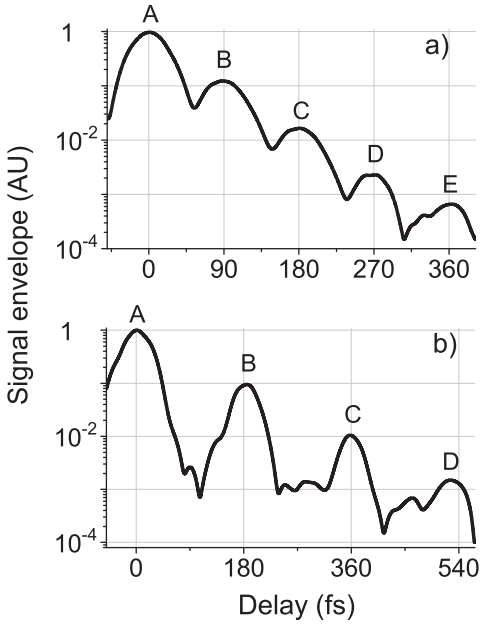

Figure 4.4. Carrier envelopes of the demodulated experimental signal for samples with slit separation equal to 25 μm (a) and 50 μm (b), respectively.

plot, on a logarithmic scale, in Fig. 4.4a. Here we see that the signal contains *five* interference maxima (peaks A–E), spanning four decades of signal. The interference maxima are equidistant with a peak-to-peak separation of 93 fs. The two additional peaks that show up in the carrier envelope (D,E) are then identified with the case that a surface plasmon is back-scattered *twice* and *three times*, respectively. Altogether, the surface plasmon is seen to make two full round trips through the cavity. Figure 4.4b shows the carrier envelope for the case that a double slit with a slit separation of 50 μm is studied. Here we observe essentially the same features as before, except that, naturally, the subsidiary maxima are farther apart and thus better resolved.

4.4 Discussion

The experimental data of Fig. 4.4 give direct access to some important experimental parameters, i.e., the SP group velocity v_{group}, the complex SP coupling factor α, and the (complex) SP amplitude reflection coefficient r. When the subsequent peaks in the interferogram are well separated and the

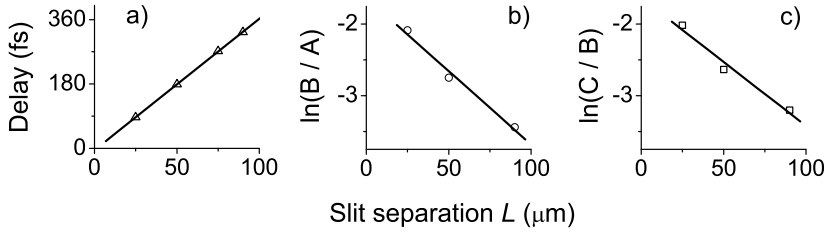

Figure 4.5. (a) Delay between peaks A (direct transmission) and B (representing the surface plasmon wavepacket) for different slit separations L. The slope of the line through the points determines the value of $1/v_{\mathrm{group}}$; (b) Ratio of the second to first peaks (B/A) as a function of the slit separation L; (c) Ratio of the third to second peaks (C/B) for different values of the slit spacing.

group-velocity dispersion of the SP is small or negligible, the group velocity can be determined directly from the separation between subsequent peaks in the signal envelope. Both v_{group} and its dispersion can be calculated from the dispersion relation of the SP travelling along the plane interface between a metal and a dielectric [8],

$$k_{\mathrm{sp}}(\omega) = \frac{\omega}{c}\sqrt{\frac{\epsilon_{\mathrm{m}}(\omega)\epsilon_{\mathrm{d}}(\omega)}{\epsilon_{\mathrm{m}}(\omega)+\epsilon_{\mathrm{d}}(\omega)}}, \tag{4.1}$$

with $\epsilon_{\mathrm{m}}(\omega)$ and $\epsilon_{\mathrm{d}}(\omega)$ the dielectric coefficients of the metal and the dielectric, respectively. We use the tabulated values for $\epsilon_{\mathrm{m}}(\omega)$ [53] and set $\epsilon_{\mathrm{d}}(\omega) = 1$, the dielectric being air. At $\lambda = 770$ nm we calculate $v_{\mathrm{group}} = \mathrm{d}\omega/\mathrm{d}k_{\mathrm{sp}} \simeq 2.72\times10^8$ m/s and a value for the group velocity dispersion $\mathrm{d}^2k_{\mathrm{sp}}/\mathrm{d}\omega^2 \simeq 0.76$ fs$^2/\mu$m equivalent to a group delay dispersion $\mathrm{d}(v_{\mathrm{group}}^{-1})/\mathrm{d}\lambda \simeq -2.4$ as/nm$\cdot\mu$m. For the experiment with a slit separation of 50 μm and the pulse spectral width $\Delta\lambda =$ 27 nm (corresponding to a Fourier-limited $\cosh^{-1}$ pulse duration of 32 fs) the group delay dispersion leads to a pulse broadening of only 5 fs and can therefore be neglected. It is therefore perfectly allowed to extract an experimental value of the SP group velocity directly from the separation between successive peaks in the interferogram (Fig. 4.5a), provided that they are well separated, as in the case of 50 μm slit separation. This yields $v_{\mathrm{group}} = 2.70 \pm 0.03 \times 10^8$ m/s. This result is in excellent agreement with the calculated value and with [73], in contrast to the findings of Bai *et al.* [83]. An experimental indication that effects of group velocity dispersion are indeed small comes from the observation that all peaks in the interferogram have the same width.

The height of the various peaks in the interferogram provides information

on both the absolute value of the light→SP→light coupling coefficient α and of the SP reflection coefficient r. The peak-height ratio (B/A) of the first echo and the peak at zero delay is given by $|\alpha| \exp(-k''_{\rm sp} L)$, while that of the second and first echo's (C/B) is given by $|r| \exp(-k''_{\rm sp} L)$. By determining these peak-height ratio's from measurements performed on double-slit systems with different inter-slit separations L, and plotting these ratio's on a logarithmic scale versus L, as shown in Fig. 4.5, we can extract $|\alpha|$ and $|r|$ from the line intercepts and $k''_{\rm sp}$ from the slope of the lines. This yields $|\alpha| = 0.19 \pm 0.02$, $|r| = 0.18 \pm 0.01$ and $k''_{\rm sp} = 0.02\ \mu{\rm m}^{-1}$. The damping constant is approximately twice the value that one calculates from the surface-plasmon dispersion relation (Eq. (4.1)) using Palik's data for the dielectric coefficient of gold [53]. We attribute the additional damping to the fact that our gold film has deteriorated over a period of a year of use, giving rise to scattering loss in the film. The value for α is in good agreement with the prediction by Lalanne *et al.* [34]. The intensity reflection coefficient $R = |r|^2$ of the slit is quite small ($R \approx 0.04$); consequently the cavity finesse is very small: $\mathcal{F} = 2.1$. Similar values for the reflection coefficients from edges and subwavelength-wide groves and barriers have been reported [84–89].

The interferogram is also sensitive to the phase of both α and r, and to illustrate that point we return to the resonator picture discussed earlier. The output of the "resonator" consists of a sequence of pulses, the first one (A) simply being the light directly transmitted through the slits, the second (B) due to the SP being excited at one slit and scattered back into light at the other slit, the third (C) due to the reflected SP being back-scattered into light at the first slit, etc. The transfer function $G(\omega)$ of the double slit can thus be written as:

$$G(\omega) = 1 + \alpha \exp[ikL] + \alpha r \exp[2ikL] + \alpha r^2 \exp[3ikL] + \cdots , \quad (4.2)$$

$$= 1 + \frac{\alpha \exp[ikL]}{1 - r \exp[ikL]}, \quad (4.3)$$

with $k = k_{\rm sp}(\omega)$ the complex surface-plasmon wave vector (see Eq. (4.1)); here the coefficients α and r are assumed to be frequency independent. In the limit that $r = 0$ this transfer function gives rise to a sinusoidally modulated two-slit spectrum [61], showing maxima whenever $kL + \arg(\alpha) = 2\pi m$, with m integer. Various theoretical studies suggest that $\arg(\alpha) = \pi$ [34, 61, 90].

Note that the transfer function of Eq. (4.2) is very similar to that describing the amplitude reflectivity of a conventional Fabry-Pérot resonator [59]:

$$\mathcal{R}(\omega) = r\left(1 - \frac{(1-r^2)\exp[2ik_0L]}{1-r^2\exp[2ik_0L]}\right). \tag{4.4}$$

For not too small values of the (real-valued) amplitude reflectivity r of the resonator mirrors, the reflectivity spectrum $|\mathcal{R}(\omega)|^2$ of a Fabry-Pérot displays deep dips whenever $2k_0L = 2\pi m'$, with m' an integer, on an otherwise constant background. These resonances occur when the denominator in Eq. (4.4) reaches its minimum value. Because of the strong similarities between Eqs. (4.2) and (4.4) we conclude that the resonances of the transmission spectrum $|G(\omega)|^2$ of our double slit appear when $kL + \arg(r) = 2\pi n$, with n an integer. The shape of the resonance (dip, peak, or asymmetric Fano-type [91]) is then determined by the phase of $\alpha\exp[ikL]$, i.e., by $u = \arg(r) - \arg(\alpha)$. When $u = 0$ the spectrum shows peaks, when $u = \pm\pi$, the spectrum carries dips, and Fano-type features arise when $u \approx \pm\pi/2$. Experimental results for the plasmon-induced modulation of the two-slit transmission spectrum hint at a value for u close to zero [61].

The transmission spectrum of the double slit (see Eq.(4.2)) plays an important role also in the time-domain response of the double slit since the interferometer signal can be written as [92]:

$$I(t) = 2\int_{-\infty}^{+\infty} |E(\omega)G(\omega)|^2\cos(\omega t)\mathrm{d}\omega, \tag{4.5}$$

with $E(\omega)$ the field incident on both slits. We assume here that our Michelson interferometer is symmetric, i.e. that the transfer functions of both interferometer arms are equal. If the spectrum of $E(\omega)$ is much broader than the separation $\Delta\Omega$ of modulation features in $G(\omega)$ (see Fig. 4.6a), the interferometer signal will approximately equal the Fourier transform of $|G(\omega)|^2$, i.e., the interferometer signal will consist of a rapidly decaying series of equidistant bursts, separated by an interval equal to L/v_{group}, representing the subsequent round trips through the cavity. The duration of these bursts (in units of pump-probe delay) is determined by the coherence time of the incident light τ_{coh}. In this limit one thus observes well separated individual pulses; Fig. 4.4b serves as an example. When the slit separation is reduced the modulation features in $G(\omega)$ lie further apart so that $E(\omega)$ and $G(\omega)$ are modulated on the same scale (see Fig. 4.6b). In that limit the interferometer signal consists of more or less overlapping peaks and, in the overlap regions is quite sensitive to the value of the parameter u, as we shall see below. The limit where the spectral width of $E(\omega)$ is much smaller than a single modulation feature of $G(\omega)$ (see

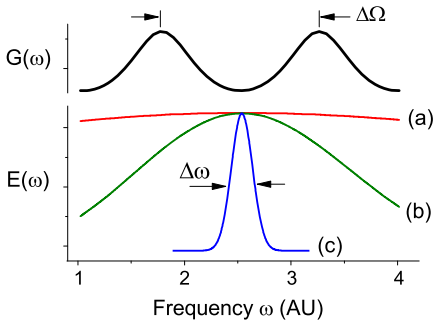

Figure 4.6. Spectral representation of the two-slit transfer function $H(\omega)$ and field $E(\omega)$ (a–c).

Fig. 4.6c) is uninteresting, corresponding to a situation where the coherence time of the incident light is much larger than the memory time of the two-slit cavity. In this limit, time-domain experiments are ineffective.

Let us now look in more detail at the intermediate regime where the coherence time τ_{coh} of the input pulse is comparable to the cavity round-trip time τ_{cav}. Let us further assume that the average frequency of the incident light is tuned so that $kL + \arg(\alpha)$ is an integer multiple of 2π (in the approximation that the surface plasmons do *not* reflect from the slits ($r = 0$), the incident light is tuned to a transmission maximum). Then the first two terms in Eq. (4.2) are in phase; in the interferometer signal the first two peaks will then add so that the dip between these peaks will be shallow. If $kL + \arg(r)$ is also an integer multiple of 2π (i.e., $u = 0$), all terms in Eq. (4.2) are in phase, so that all neighboring peaks in the interferogram are separated by shallow dips (see Fig. 4.7a). If, however, $kL + \arg(r)$ is an odd multiple of π ($u = \pi$), each subsequent term in Eq. (4.2) is out of phase with the previous one giving rise to deep dips between second, third, fourth, fifth etc. peaks in the interferogram (see Fig. 4.7b).

If, however, we tune the laser so that $kL + \arg(\alpha)$ is an odd multiple of π the first two terms in Eq. (4.2) are out of phase and give rise to a deep dip between the first two peaks in the interferogram. If now $kL + \arg(r)$ is an integer multiple of 2π (so that $u = \pi$) the subsequent terms in Eq. (4.2) will all be in phase with each other giving rise to shallow dips between peaks $2, 3, 4, \ldots$ in the interferogram (see Fig. 4.7c). If, however, $kL + \arg(r)$ is an odd multiple of π (so that $u = 0$) all subsequent terms in Eq. (4.2) will all be out of phase with each other giving rise to deep dips between all peaks in the interferogram (see Fig. 4.7d). Figures 4.7e and 4.7f show experimental results obtained for

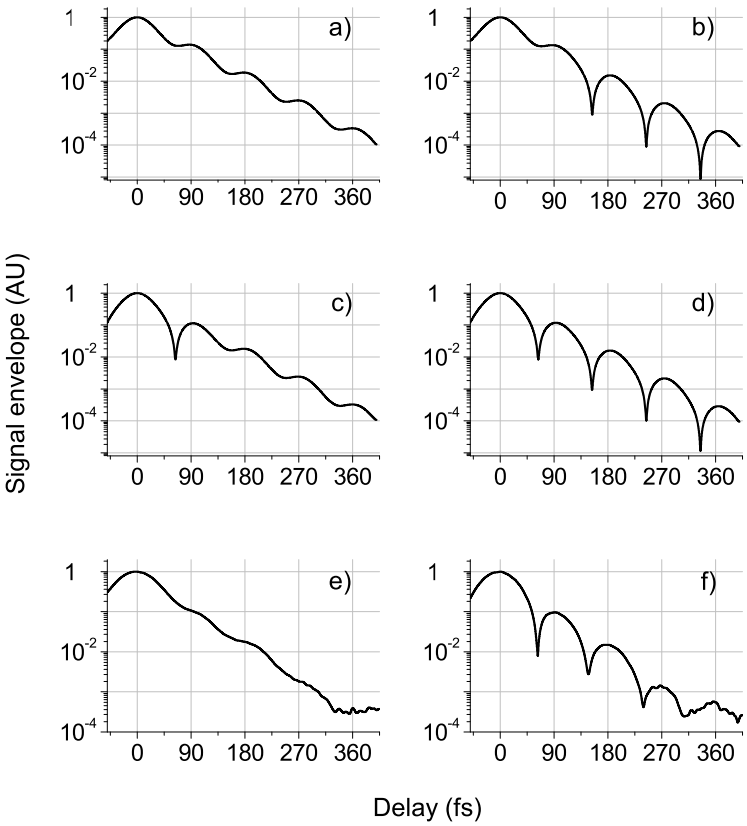

Figure 4.7. Calculated and experimental interferograms for various values of the tuning of the laser wavelength. Frames a) and d) show calculated data for the case that the phase parameter $u = 0$, while frames b) and c) show such data for the case that $u = \pi$. Frames e) and f) show experimental results for two different wavelength settings of the laser: in e) the laser is tuned to a transmission maximum; in f) to a transmission minimum.

the 25 μm slits at two different settings of the laser, one corresponding to the case $kL + \arg(\alpha) = 2m\pi$ (Fig. 4.7e) and one corresponding to the case $kL+\arg(\alpha) = (2m+1)\pi$ (Fig. 4.7f). These experimental results clearly suggest that $u \approx 0$.

This value for the parameter u fits well with the shape of the transmission spectrum of the double slit, as measured with TM-polarized incident light. Figure 4.8 shows such a spectrum together with spectra calculated on the basis that $|\alpha| = |r| = 0.2$, one spectrum for the case that $u = 0$, the other

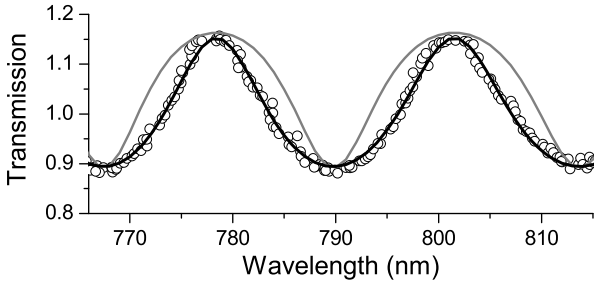

Figure 4.8. Double-slit transmission spectrum for TM-polarized incident light. The circles show the experimental data, the solid lines calculated spectra for $|\alpha| = |r| = 0.2$. The black line shows the result for $u = 0$, while the gray line represents a $u = \pi$ spectrum.

for the case $u = \pi$. Clearly, the curve with $u = 0$ provides a much better description of the experimental data than that with $u = \pi$.

4.5 Conclusions

In summary, we have used a high-dynamic range time-domain technique to investigate the propagation and scattering of surface plasmons as they travel between two sub-wavelength slits along the interface between air and a smooth gold film. With slit distances of the order of the surface-plasmon damping length, i.e. tens of micrometers, we have measured the group velocity of the surface plasmon and found it to be in excellent agreement with the value calculated from the dispersion relation using Palik's tabulated values for the dielectric properties of gold in the near-infrared spectral region. Furthermore, we have determined the magnitude of the surface-plasmon scattering and reflection coefficients upon interaction with the sub-wavelength slits. The magnitude of the scattering coefficient, describing the second-order process where incident light is scattered into a surface-plasmon which, in turn, is scattered into diffracted light, is in good agreement with the value recently calculated by Lalanne *et al.* [35]. The measured value of the reflection coefficient agrees well with theoretical calculations [24,88] and experimental data obtained with somewhat different nano-structured surfaces [85, 87]. Finally, we have determined that the scattering and reflection coefficients have roughly equal phase. The latter result allows us to explain fine details in the transmission spectrum of the double slit that have, hitherto, gone unnoticed.

4.6 Appendix: Slowed-down surface plasmons (unpublished)

The dispersion of a surface plasmon that propagates along a metallo-dielectric interface is sensitive to the dielectric permittivity ϵ_d of the dielectric (see Fig. 4.9). Consequently, the group velocity, given by the tangent to the dispersion curve at a specific value of ω, is also sensitive to the dielectric's permittivity. Here we present some experimental results that probe that dependence.

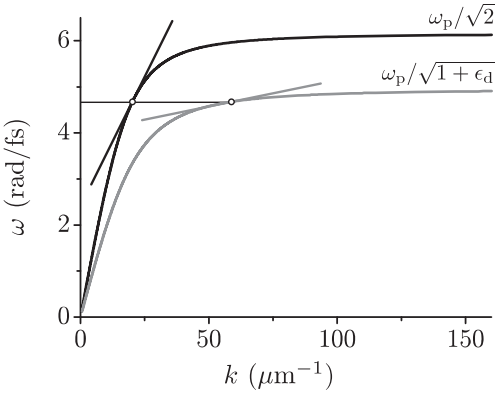

Figure 4.9. Dispersion relation for a surface plasmon traveling along a smooth interface between a metal and air (dark solid line) and between a metal and a dielectric with permittivity ϵ_d (light solid line).

We use the experimental arrangement of the foregoing Chapter, using a laser emitting transform-limited 100 fs pulses at $\lambda = 800$ nm. We illuminate the sample from the metallic side and probe the 90 μm double slit that is milled in the gold film. Consecutively, we deposit thin layers of methanol, ethanol and acetone on the sample and measure the group velocity of the surface plasmons traveling between the slits. At $\lambda = 800$ nm the refractive indices of these liquids at room temperature (20 °C) are $n = 1.3290$ (methanol), $n = 1.3614$ (ethanol) and $n = 1.3590$ (acetone), respectively. The thickness of the liquid layer is chosen to be so large that the (phantom) peaks in the interferogram arising from multiple reflections between the air-liquid and liquid-gold interfaces are outside our range of interest.

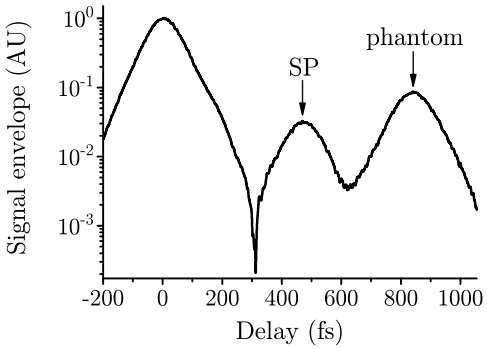

Figure 4.10. Envelope of the interferogram arising from the gold-ethanol interface for two slits that are 90 μm apart.

The experimental data for the gold-ethanol interface are shown in Fig. 4.10. Apart from the peak at zero delay one distinguishes a peak associated with the surface-plasmon traveling between the slits (labeled SP) and a phantom peak associated with reflections of the incident light in the thin layer of liquid. Since the various peaks in the interferogram are well separated we can immediately deduce a value for the surface-plasmon group velocity at $\lambda_{\text{inc}} = 800$ nm on the gold-liquid interface. The results are collected in Table 4.1, together with values for the group velocity calculated with the dispersion diagram. The agreement is excellent.

Dielectric	Measured group velocity (m/s)	Calculated group velocity (m/s)
Methanol	$1.97 \pm 0.04 \times 10^8$	1.96×10^8
Ethanol	$1.93 \pm 0.04 \times 10^8$	1.90×10^8
Acetone	$1.97 \pm 0.04 \times 10^8$	1.90×10^8
Air	$2.70 \pm 0.03 \times 10^8$	2.72×10^8

Table 4.1. Values of the group velocity of a surface plasmon traveling along a gold-dielectric interface for various dielectric materials. The experiments were performed at $\lambda = 800$ nm.

Interestingly, the experimental data of Fig. 4.10 show a very pronounced dip between the peak at zero delay and the peak associated with the surface plasmon, indicating that, in this experiment, the center of the laser spectrum is very well aligned with a transmission *minimum* of the double-slit transmission function.

We have tried to extend these measurements to liquids such as benzyl-alcohol, which have a higher refractive index $n \simeq 1.54$. These, however, were unsuccessful. Probably, in these cases, the liquid layer formed a wedge so that, effectively, the sample was tilted. As discussed in the Appendix to Chapter 2, the plasmonic interference effects can easily be washed out in that case.